Eur. Phys. J. A **27**, 157–165 (2006)
DOI 10.1140/epja/i2005-10259-y

THE EUROPEAN PHYSICAL JOURNAL A

Gamma-ray spectroscopy of the doubly magic nucleus ^{56}Ni

E.K. Johansson[1,a], D. Rudolph[1], J. Ekman[1,b], C. Fahlander[1], C. Andreoiu[1,c], M.A. Bentley[2,d], M.P. Carpenter[3], R.J. Charity[4], R.M. Clark[5], P. Fallon[5], R.V.F. Janssens[3], F.G. Kondev[3], T.L. Khoo[3], T. Lauritsen[3], A.O. Macchiavelli[5], W. Reviol[4], D.G. Sarantites[4], D. Seweryniak[3], C.E. Svensson[5,c], and S.J. Williams[2,e]

[1] Department of Physics, Lund University, S-22100 Lund, Sweden
[2] School of Chemistry and Physics, Keele University, Keele, Staffordshire ST5 5BG, UK
[3] Physics Division, Argonne National Laboratory, Argonne, IL 60439, USA
[4] Chemistry Department, Washington University, St. Louis, MO 63130, USA
[5] Nuclear Science Division, Lawrence Berkeley National Laboratory, Berkeley, CA 94720, USA

Received: 20 December 2005 / Revised version: 31 January 2006 /
Published online: 27 March 2006 –
Communicated by R.K. Krücken

Abstract. The doubly magic $N = Z$ nucleus ^{56}Ni has been investigated with two fusion-evaporation reactions; ^{40}Ca(^{28}Si, 3α)^{56}Ni at a beam energy of 122 MeV and ^{28}Si(^{32}S, 2p2n)^{56}Ni at 130 MeV. To detect γ-rays in coincidence with evaporated particles the Ge-detector array Gammasphere was used in conjunction with the charged-particle detector system, Microball and a 1π neutron detector array. Results include a significantly extended level scheme of ^{56}Ni, which is compared to large-scale shell model calculations in the fp shell. The experimental and theoretical results agree to a large extent, with one notable exception; the theoretical model fails to predict the proper sequence of the yrast and yrare 8^+ states.

PACS. 21.60.Cs Shell model – 23.20.En Angular distribution and correlation measurements – 23.20.Lv γ transitions and level energies – 27.40.+z $39 \leq A \leq 58$

1 Introduction

Fundamental building blocks within nuclear structure are the experimentally observed shell gaps associated with the magic numbers, which are very well reproduced by the nuclear shell model. In this model the $N = Z = 28$ nucleus ^{56}Ni is the first doubly magic nucleus to be described by the inclusion of the spin-orbit force in the nuclear mean-field potential. The spin-orbit force causes a splitting within the fp shell: the energetically favoured $j = \ell + s$ orbit $1f_{7/2}$ separates from the $2p_{3/2}$, $1f_{5/2}$, and $2p_{1/2}$ orbitals, also called the upper fp shell, thus, creating the shell gap at particle number 28. Consequently, the expected leading ground-state configuration of ^{56}Ni has all orbitals filled up to and including the $1f_{7/2}$ orbit. However, the probability for this ground-state configuration was found to range from some 50–70% in contemporary shell model approaches, depending on the interaction used [1]. These values are substantially lower than the corresponding numbers for the nearby doubly magic nucleus ^{48}Ca (94%), which has been taken as a sign of ^{56}Ni representing a rather soft doubly magic core [1].

Other signatures of a double shell closure include a high excitation energy of the first 2^+ state and a low quadrupole excitation strength to that state. The energy of the first 2^+ state in ^{56}Ni is established at 2.7 MeV. Though this energy is reasonable for single-particle excitations, it is relatively low compared to other doubly magic nuclei. For example, the first 2^+ state in ^{48}Ca is located at 3.8 MeV. The reduced transition strength has been measured to be $B(E2; 0^+ \rightarrow 2^+) \simeq 560\ e^2\,\mathrm{fm}^4$ via proton scattering [2] and intermediate-energy Coulomb excitation [3,4]. Contemporary shell model calculations [1] predict $B(E2; 0^+ \rightarrow 2^+) = 550\ e^2\,\mathrm{fm}^4$, *i.e.*, perfect agreement between theory and experiment. With respect to the much lower value of $B(E2; 0^+ \rightarrow 2^+) = 84\ e^2\,\mathrm{fm}^4$ in ^{48}Ca this is yet another hint for the softness of the ^{56}Ni core.

The question to be addressed in this study is whether or not this degree of consensus remains for the complete set of experimentally known states in ^{56}Ni. Early experimental work on ^{56}Ni includes an in-beam γ-ray spectroscopic study [5], establishing the yrast sequence up to

[a] e-mail: emma.johansson@nuclear.lu.se
[b] *Present address:* Malmö högskola, S-20506 Malmö, Sweden
[c] *Present address:* Department of Physics, University of Guelph, Guelph, Ontario, Canada N1G 2W1.
[d] *Present address:* Department of Physics, University of York, Heslington, York, YO10 5DD, UK.
[e] *Present address:* School of Chemistry and Physics, University of Surrey, Guildford, Surrey GU2 7XH, UK.

a tentative spin and parity of $I^\pi = 10^+$. A subsequent high-spin study of ^{56}Ni led to the discovery of two superdeformed rotational structures [6]. While one band can readily be explained by Hartree-Fock–based mean-field models *and fp* shell model calculations, the second band requires the excitation of one particle into the $1g_{9/2}$ intruder orbital [6–8].

In this paper results from two data sets are combined. This more than doubles the number of known γ-ray transitions and excited states in ^{56}Ni. The experimental data are compared with the results of a large scale, state-of-the-art shell model calculation. In particular, electromagnetic decay properties are investigated in detail, revealing deficiencies in the theory to properly describe all yrast states in ^{56}Ni.

2 Experiment and data analysis

Excited states in ^{56}Ni were studied with two different heavy-ion fusion-evaporation reactions initiated at the 88″ cyclotron at Lawrence Berkeley National Laboratory and at the ATLAS facility at Argonne National Laboratory.

Experiment 1 utilized a ^{28}Si beam with an energy of 122 MeV impinging on a 0.5 mg/cm^2 thin ^{40}Ca target, creating a compound nucleus of ^{68}Se. Through emission of 3α particles, ^{56}Ni is obtained. The 99.98% enriched target foil was sandwiched between two thin layers of gold to prevent oxidation. The γ-rays were detected in the Gammasphere array [9], which comprised 101 Compton-suppressed Ge-detectors with the Heavimet collimators removed. This allows for γ-ray multiplicity and sum-energy measurements. Evaporated light charged particles were detected with the 4π CsI-array Microball [10]. Events were collected if four or more Compton-suppressed γ-rays were detected. For further information on the experiment see ref. [11].

In experiment 2, a beam of ^{32}S collided with a ^{28}Si target foil at a beam energy of 130 MeV. This reaction produced the compound nucleus ^{60}Zn, which generates ^{56}Ni by emission of two protons and two neutrons. The 0.5 mg/cm^2 thin ^{28}Si target was enriched to 99.90% and supported either with 1.0 mg/cm^2 Au or 1.0 mg/cm^2 Ta facing the 130 MeV ^{32}S beam. The energy loss in the foil amounts to 5 MeV, thus the effective beam energy was 125 MeV. Here the Gammasphere comprised 78 Ge-detectors with the Heavimet collimators removed as well. Microball was used to measure and identify light charged particles. The five most forward rings of Gammasphere were replaced by the Neutron Shell [12], consisting of 30 liquid scintillator detectors to enable neutron detection. The trigger used was either four or more γ-rays in coincidence, or three or more γ-rays in coincidence with one or more pre-discriminated neutrons. More details can be found in ref. [13].

In the analysis of both experiments, discrimination between protons and α particles is crucial in creating clean particle gated spectra with sufficient statistics. Therefore, each Microball event was associated with time, energy, and charge-ratio signals [10] obtained through pulse shape techniques. These signals were plotted in three two-dimensional spectra, and particles were identified only after fulfilling gate conditions in all three maps. Subsequently, the γ-ray energy resolution was optimized by an event-by-event kinematic reconstruction method to reduce the effect of the Doppler broadening due to the evaporated particles.

To distinguish between neutron- and γ-ray signals from the neutron detectors, pulse shape discrimination techniques were utilized. Four signals from each neutron detector were digitized: time of flight (TOF), zero-cross-over time (ZCO), energy, and the tail of the energy signal [12]. Two-dimensional gates on several combinations of these signals provided a clean distinction between neutrons and γ-rays [9,12].

In both experiments, the events were sorted off-line into E_γ-E_γ correlation matrices. These were subject to appropriate evaporated particle conditions, *i.e.*, the γ-rays had to be in coincidence with three α particles (3α) for experiment 1, and with two protons and two neutrons (2p2n) for experiment 2.

The main contaminating reaction channels in the γ-ray spectra are those for which one proton escaped detection, namely, the 3p2n and 3α1p channels, respectively, leading to the well-known isotope ^{55}Co in both cases. Some contaminations from the 2p1n and 3p1n channels (^{57}Ni and ^{56}Co) were also present in the 2p2n selected γ-ray spectra from experiment 2. This is due to the remaining one-neutron scattering events, which can mimic two-neutron events, but unfortunately passed the two-neutron selection criteria [13]. In experiment 1, possible misidentification of two protons as one α particle results in the inclusion of ^{58}Ni created in the 2α2p evaporation channel, as can be seen in fig. 3. Nevertheless, all these contaminations can easily be handled or eliminated by studying γ-ray matrices and spectra in coincidence with the respective number and type of evaporated light particles. The analysis employed the Radware software package [14] and the Cologne spectrum analysis code Tv [15].

The spins and parities of the states were determined by utilizing yields measured by Ge detectors placed at different angles with respect to the beam axis. In experiment 1, 15 detectors at forward and 15 detectors at backward angles were combined to create a "pseudo" ring at an effective angle of 30°. Similarly, 28 detectors between 80° and 100° make up a "pseudo" ring placed at an average angle of 83°. This is based on the fact that the angular distribution of γ-rays is symmetric with respect to the reaction plane. Particle-gated $\gamma\gamma$ matrices with γ-rays detected at 30° (alteratively 83°) *vs.* γ-rays detected anywhere in the array were generated. From these matrices the intensity ratios

$$R_{30\text{–}83} = \frac{I_\gamma(30^\circ)}{I_\gamma(83^\circ)} \quad (1)$$

can be obtained [16]. These allow the deduction of spin and parity for the excited states, as γ-rays of different multipolarities have different angular distributions and, hence $R_{30\text{–}83}$ values. Stretched quadrupole transitions are predicted to have $R_{30\text{–}83} \sim 1.3$, whereas an $R_{30\text{–}83} \sim 0.8$

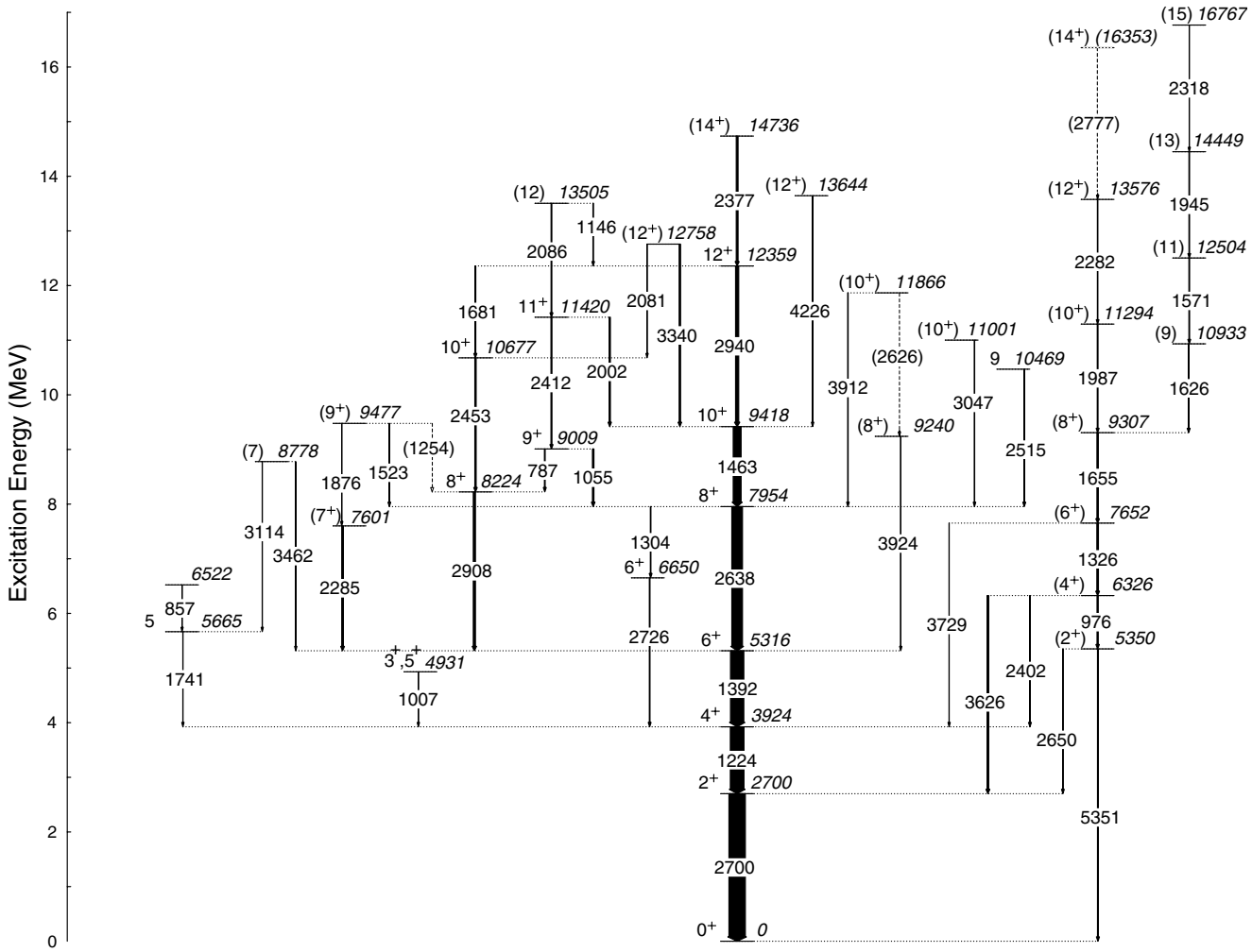

Fig. 1. The proposed experimental level scheme of ^{56}Ni from the present work, featuring some 20 new transitions. The energy labels are given in keV. The widths of the arrows are proportional to the relative intensities of the γ-rays. Dashed lines indicate tentative transitions and states.

indicates a stretched dipole transition. Significant deviations from the latter values indicate $E2/M1$ mixing, which in some cases allows parity to be assigned.

3 Results

The level scheme resulting from the present analysis is displayed in fig. 1. The number of observed γ-rays and excited states have roughly doubled the experimental knowledge of ^{56}Ni with respect to ref. [6]. The transitions and their placement in the level scheme have been determined by $\gamma\gamma$ coincidences, sum-energy relations of transitions, and their relative intensities. Spins and parities of the states have been determined from the R_{30-83} ratios and yrast state considerations. They are summarized in table 1.

All four γ-ray spectra shown in figs. 2, 3, 4, and 5 originate from the 3α-gated $\gamma\gamma$-matrix from experiment 1. The spectrum in fig. 2 is obtained by gating on the 2700, 1224, and 1392 keV transitions in the $\gamma\gamma$-matrix, and summing their contributions. The established [16] irregular yrast sequence of 2700, 1224, 1392, 2638, 1463, 2940, and 2377 keV

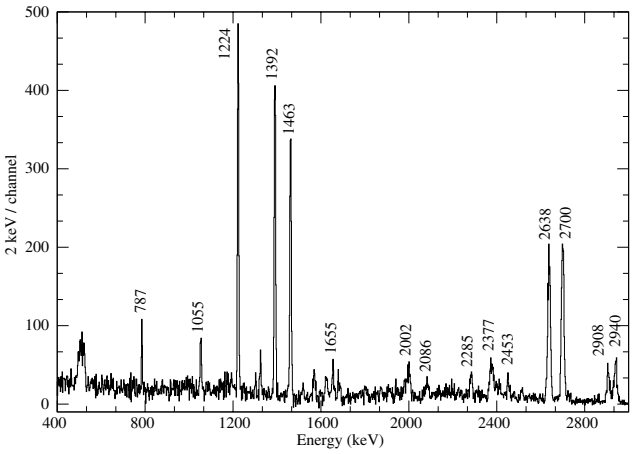

Fig. 2. Spectrum of ^{56}Ni created by gating on the intense transitions in the $6^+ \rightarrow 4^+ \rightarrow 2^+ \rightarrow 0^+$ yrast cascade, in a 3α-gated $\gamma\gamma$ coincidence matrix.

transitions is clearly seen. A new odd-spin structure starts from the 9^+ state at 9009 keV. It decays by two transitions

Table 1. The energies of the excited states in ^{56}Ni, as well as the energies and relative intensities of the γ-rays placed in the level scheme, their angular distribution ratios and multipole assignments, and to the very right the spins and parities of initial and final states.

E_{exc} (keV)	E_γ (keV)	I_{rel}[a] (%)	I_{rel}[b] (%)	R_{30-83}[a]	R_{30-83}[b]	Mult. ass.	I_i^π ($\hbar$)	I_f^π ($\hbar$)
2700(1)	2700(1)	100(4)	100(4)	1.3(1)	1.2(1)	$E2$	2^+	0^+
3924(1)	1224(1)	83(3)	100(3)	1.3(1)	1.3(1)	$E2$	4^+	2^+
4932(2)	1008(1)	—	4.7(5)	—	0.4(2)	$E2/M1$	3^+,5^+	4^+
5316(1)	1392(1)	81(4)	69(3)	1.4(1)	1.4(1)	$E2$	6^+	4^+
5350(1)	2650(1)	3.3(8)	—	—	—	$\Delta I = 0$	2^+[c]	2^+
	5351(2)	5.3(4)	—	1.6(1)	—	$E2$	2^+	0^+
5665(1)	1741(1)	—	7.9(8)	—	0.6(2)	$\Delta I = 1$	5	4^+
6326(1)	976(1)	7.4(18)	—	—	—	$(E2)$	(4^+)[c]	2^+
	2402(1)	4.3(21)	—	—	—	$(\Delta I = 0)$	(4^+)	4^+
	3626(1)	10(2)	—	—	—	$(E2)$	(4^+)	2^+
6522(2)	857(1)	—	3.8(4)	—	—	—	—	5
6650(1)	2726(1)	4.1(7)	5.8(12)	1.4(4)	1.2(4)	$E2$	6^+	4^+
7601(2)	2285(1)	10(2)	7.3(13)	$\gg 1$	$\gg 1$	$(E2/M1)$	(7^+)	6^+
7652(1)	1326(1)	9.5(34)	—	—	—	$(E2)$	(6^+)[c]	(4^+)
	3729(2)	0.8(4)	—	—	—	$(E2)$	(6^+)	(4^+)
7954(1)	1304(1)	3.5(5)	2.6(4)	1.3(3)	—	$E2$	8^+	6^+
	2638(1)	65(3)	31(2)	1.3(1)	1.4(2)	$E2$	8^+	6^+
8224(2)	2908(1)	13(1)	12(1)	1.3(1)	1.0(2)	$E2$	8^+	6^+
8778(2)	3114(2)	—	< 1	—	—	—	(7)	5
	3462(1)	< 1	2.1(4)	—	—	—	(7)	6^+
9009(2)	787(1)	4.5(6)	5.9(5)	0.6(1)	—	$E2/M1$	9^+	8^+
	1055(1)	8.8(8)	7.2(6)	0.5(1)	0.7(2)	$E2/M1$	9^+	8^+
9240(2)	3924(2)	—	1.5(4)	—	—	$(E2)$	(8^+)	6^+
9307(2)	1655(1)	8.4(34)	—	—	—	—	(8^+)[c]	(6^+)
9418(2)	1463(1)	48(3)	17(1)	1.4(1)	1.4(2)	$E2$	10^+	8^+
9477(2)	1254(2)	1.2(7)	—	—	—	—	(9^+)	8^+
	1523(1)	2.1(5)	2.1(4)	1.6(3)	1.4(4)	$(E2/M1)$	(9^+)	8^+
	1876(2)	< 1	1.4(4)	—	—	—	(9^+)	(7^+)
10469(2)	2515(1)	4.4(7)	2.1(8)	0.6(2)	1.0(3)	$\Delta I = 1$	9	8^+
10677(2)	2453(1)	8.0(9)	4.1(6)	1.1(2)	1.5(4)	$E2$	10^+	8^+
10933(2)	1626(1)	4.6(9)	—	—	—	—	(9)[c]	(8^+)
11001(2)	3047(1)	2.0(5)	—	—	—	$(E2)$	(10^+)	8^+
11294(2)	1987(1)	4.6(22)	—	—	—	—	(10^+)[c]	(8^+)
11420(2)	2002(1)	7.6(10)	3.7(16)	1.6(5)	$\gg 1$	$E2/M1$	11^+	10^+
	2412(1)	5.8(11)	3.2(6)	0.9(1)	—	$E2$	11^+	9^+
11866(2)	2626(2)	< 1	—	—	—	—	(10^+)	(8^+)
	3912(2)	2.8(6)	< 1	1.0(3)	—	$(E2)$	(10^+)	8^+
12359(2)	1681(1)	5.4(6)	2.6(5)	1.2(2)	—	$E2$	12^+	10^+
	2940(1)	19(2)	5.1(7)	1.5(1)	1.2(3)	$E2$	12^+	10^+
12504(2)	1571(1)	4.2(9)	—	—	—	—	(11)[c]	(9)
12758(2)	2801(1)	1.7(7)	—	—	—	—	(12^+)	10^+
	3340(1)	8.4(9)	—	1.6(3)	—	$(E2)$	(12^+)	10^+
13505(2)	1146(1)	2.8(5)	—	0.8(2)	—	$\Delta I = 0$	(12)	12^+
	2086(1)	4.6(7)	2.6(5)	0.8(3)	—	$\Delta I = 1$	(12)	11^+
13576(2)	2282(1)	2.8(14)	—	—	—	—	(12^+)[c]	(10^+)
13644(3)	4226(2)	1.2(5)	—	—	—	—	(12^+)	10^+
14449(2)	1945(1)	3.7(8)	—	—	—	—	(13)[c]	(11)
14736(2)	2377(1)	11(3)	—	1.1(1)	—	$(E2)$	(14^+)	12^+
16353(3)	2777(2)	< 1	—	—	—	—	(14^+)	(12^+)
16767(3)	2318(2)	< 1	—	—	—	—	(15)[c]	(13)

[a] Data from experiment 1; ^{40}Ca(^{28}Si, 3α)^{56}Ni.

[b] Data from experiment 2; ^{28}Si(^{32}S, 2p2n)^{56}Ni.

[c] Data taken from ref. [16].

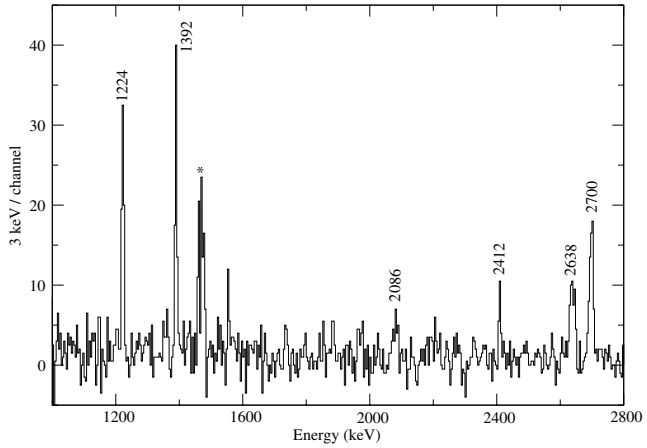

Fig. 3. Spectrum in coincidence with the 1055 keV, $9^+ \rightarrow 8^+$ transition, showing the new odd-spin structure. The peak marked with a star is the $2^+ \rightarrow 0^+$ ground-state transition in the contaminating ^{58}Ni nucleus.

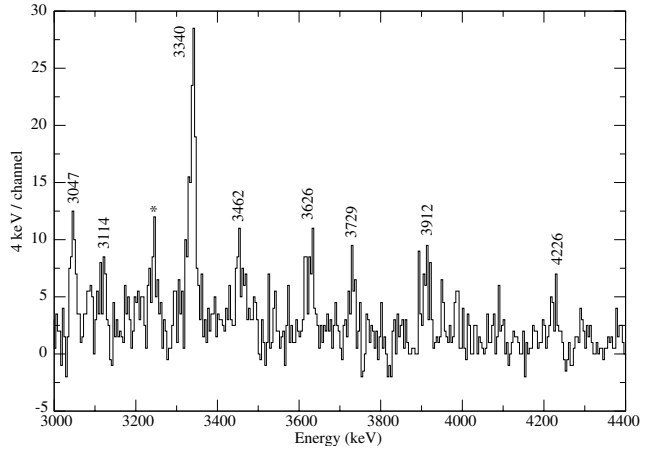

Fig. 4. High-energy portion of fig. 2, showing some high-energy transitions. The 3246 keV peak, marked with a star, could not be placed in the level scheme.

of 787 and 1055 keV, which are also clearly visible in fig. 2. The level at 9009 keV is determined to be a 9^+ state due to the R_{30-83} ratios of the 787 and 1055 keV transitions, which feed into 8^+ states and both R_{30-83} indicate a mixed $E2/M1$ character.

Figure 3 displays the spectrum in coincidence with the new $9^+ \rightarrow 8^+$1055 keV transition. The yrast sequence from the 8^+ level towards the ground state is clearly seen. The new $11^+ \rightarrow 9^+$ transition of 2412 keV and the 2086 keV transition feeding into the 11420 keV 11^+ state are also visible in fig. 3. The R_{30-83} ratio of the 2086 keV transition indicates that it originates from a state with spin 12, while no parity can be assigned.

A difficulty in assigning spin and parity to states of high excitation energy exists if the state decays very rapidly, *i.e.*, for states having very short effective lifetimes. If the ^{56}Ni nuclei decay while still inside the target, the Doppler corrections will not work properly. This affects the spectra from the Ge pseudo ring at 30° more than the

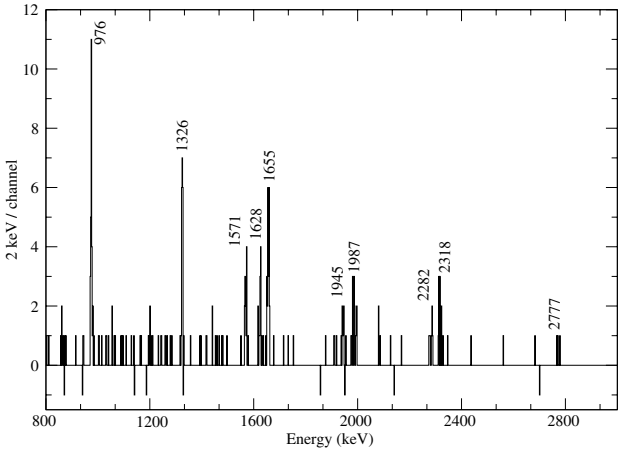

Fig. 5. Spectrum in coincidence with the 5351 keV ground-state transition. The known rotational band is clearly seen, together with a tentative 2777 keV transition. The 2318 keV transition belongs to a deformed rotational band [6].

spectra obtained from the ring at 83°, potentially leading to a reduced R_{30-83} ratio. This may, for instance, explain the relatively low R_{30-83} values of the 2412 keV $11^+ \rightarrow 9^+$ and the 2086 keV (12) $\rightarrow 11^+$ transitions. Note that a possible 10^+ assignment to the 11420 keV level is rejected based on yrast arguments, while a 12^+ assignment is impossible due to the 2412 keV connection to the 9009 keV 9^+ state. The yrast argument takes into consideration the relative intensities of the transitions. If the 11420 keV state were the fifth 10^+ state, it would have been populated less in the course of the fusion-evaporation process, *i.e.*, the intensities of the depopulating 2002 and 2412 keV transitions should have been much lower.

Several high-energy transitions attributed to ^{56}Ni are displayed in fig. 4, which represents a close up of the high-energy fraction of the spectrum shown in fig. 2. Two of the marked transitions with an energy of 3114 and 3462 keV decay from the same 8778 keV level. Due to their low statistics a tentative spin of 7 is assigned based on yrast arguments and the fact that the two transitions feed levels with spin $I = 5$ and $I = 6$, respectively. Also seen in fig. 4 is the new 3912 keV transition which decays from a tentative 10^+ state, with a level energy of 11866 keV. This state may also connect to the 9240 keV (8^+) level via the possible 2626 keV transition, which is difficult to establish because of the intense 2638 keV $8^+ \rightarrow 6^+$ transition being so close in energy. In turn the 9240 keV level decays with an 3924 keV $E2$ transition to the yrast 6^+ state.

By gating on the 5351 keV ground-state transition the spectrum shown in fig. 5 was obtained. Although the statistics in fig. 5 are very low, the spectrum is extremely clean, and the known rotational bands [6] can be seen as well as a small indication of a tentative $14^+ \rightarrow 12^+$ transition at 2777 keV. The two bands are basically not seen in experiment 2, producing ^{56}Ni in the 2p2n channel. This is because here ^{56}Ni is populated on average at somewhat lower excitation energies and spin than in experiment 1, which is reflected in the different relative

intensities given in table 1. This can be illustrated by the new low-lying 1741 keV transition. In experiment 2, this transition is quite strong with an intensity of 7.9(8)% relative to the ground-state transition. However, no indication of its presence could be found in experiment 1, as higher-lying states are preferably populated, and the decay feeds into the yrast states, which implies that this level is bypassed.

The experimentally found level at 4932 keV decays with a 1008 keV γ-ray, whose angular-distribution ratio corresponds to a mixed $E2/M1$ transition. This gives the 4932 keV level a spin of either 3 or 5, with positive parity (see table 1), while it has an $I^\pi = 3^-$ assignment in a current nuclear data base [17]. A recent β-decay study on ^{56}Cu, however, is consistent with the present result, providing $I^\pi = (3^+)$ for the 4932 keV state [18]. Note that in our data there are only indications of the 2234 keV $(3^+) \rightarrow 2^+$ branch observed in parallel to the 1008 keV decay in ref. [18] due to limited statistics.

4 Shell model interpretation

To discuss the results from the present experiments a large-scale shell model calculation was performed using the shell model code ANTOINE [19,20]. The calculation was performed using the GXPF1 interaction, which has recently been developed for the ^{56}Ni region [1,21]. Small effects from single-particle energies and two-body matrix elements arising from the Coulomb interaction have not been considered. The full fp space was utilized, including the $1f_{7/2}$ orbital below the $N = Z = 28$ shell gap, and the $2p_{3/2}$, $1f_{5/2}$, and $2p_{1/2}$ above it. The configuration space allowed up to 6p-6h excitations from the $1f_{7/2}$ shell into the upper fp shell. The choice of 6p-6h excitations is necessary and sufficient to describe the rotational band and the softness of the ^{56}Ni core including the $B(E2; 0^+ \rightarrow 2^+)$ value [6,8,22]. Electromagnetic decay properties were derived using bare g-factors and effective charges of $0.5e$ for the neutrons and $1.5e$ for the protons. Since Coulomb effects were neglected, the calculated wave functions for states in ^{56}Ni are fully symmetric in terms of proton and neutron partitions. Therefore, the use of standard effective charges is in line with recent more elaborate results on effective charges in the mass region [23].

Figure 6 compares the experimental level energies with the calculated energy eigenvalues. On the left-hand side even- and odd-spin yrast states are shown, followed by a selection of yrare states. On the very right some third and fourth states for a given spin-parity combination are presented. The overall agreement is good: the mean level deviation (MLD) amounts to 317 keV and the binding energy shift (BES) is 247 keV. The latter has been added to all calculated energy levels in fig. 6. The BES and MLD were calculated by including all levels except those in the rotational band.

If the yrast levels were exclusively considered, a MLD value of 254 keV and a BES of 236 keV are obtained. This implies that yrare and yrast energies are almost equally well described within the model.

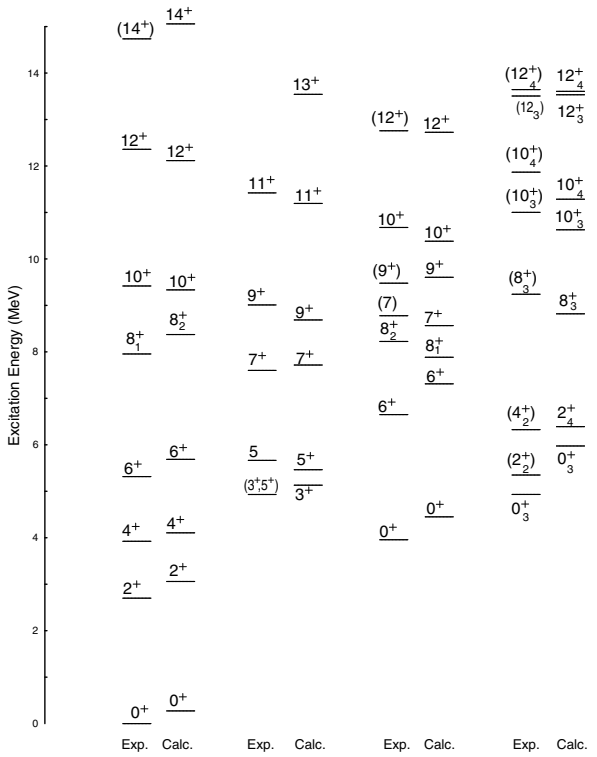

Fig. 6. The experimental and calculated excitation energies for the states observed in ^{56}Ni. From left to right: the even-spin yrast states, the odd-spin yrast states, the yrare even- and odd-spin states, to the very right higher-order even- and odd-spin states. A binding energy shift of 247 keV is added to all calculated levels. Note that the yrast experimental 8^+ is associated with the second calculated 8^+ state and vice versa.

To go beyond the standard comparison between experimental results and shell model predictions, electromagnetic decay properties were investigated. We used the effective operators mentioned earlier and the experimental γ-ray energies to infer reduced $B(M1)$ and $B(E2)$ transition rates and subsequently mixing ratios, $\delta(E2/M1)$, branching ratios, b, as well as state lifetimes, τ. The experimentally known $B(E2; 0^+ \rightarrow 2^+) \simeq 560\ e^2\,\mathrm{fm}^4$ makes it possible to calculate the lifetime for the 2^+ state to $\tau = 0.05(1)$ ps. Comparing this number with the calculated value in table 2 a good agreement is found.

From our experimental data, relative strengths can be studied by means of branching ratios. The experimental and theoretical values are presented in table 2. In the calculation all possible decay branches were studied, even if the final state is experimentally unknown or not observed in the present study. For instance, the calculated 2^+_4 state, which corresponds to the yrare 2^+ experimental level at 5350 keV [6], can decay into the ground state 0^+_1, to the known but non-observed 0^+_2 and 0^+_3 states [17], and the calculated but unknown 2^+_2 and 2^+_3 states. Table 2 includes only the most significant subset of possible final states. The evaluation is from top to bottom of the level scheme, alike the experimental de-excitation, *i.e.* the yrast experimental 14^+ was connected with the calculated 14^+_1 level, and if the theoretical and experimental branching

Table 2. Comparison of the experimental and theoretical branching ratios, b, of γ-rays in ^{56}Ni. The γ-ray energies given in italic style indicate transitions not observed (*n.o.*) in this study. See text for further details.

E_{exc} (keV)	I_i^π ($\hbar$)	I_f^π ($\hbar$)	E_γ (keV)	b_{exp}	b_{theo}	τ_{theo} (ps)
2700	2_1^+	0_1^+	2700	1.0	1.0	0.04
3924	4_1^+	2_1^+	1224	1.0	1.0	3.1
4932	3_1^+	2_1^+	*2232*	*n.o.*	0.26	6.9
		4_1^+	1008	1.0	0.74	
4936[a]	3_1^+	2_1^+	2235[a]	0.37(11)	0.26	
		4_1^+	1010[a]	0.63(11)	0.74	
5316	6_1^+	4_1^+	1392	1.0	1.0	2.4
5350	2_4^+	0_1^+	5351	0.62(6)	0.50	0.04
		0_2^+	*1393*	*n.o.*	0.29	
		2_1^+	2650	0.38(6)	0.21	
5665	5_1^+	3_1^+	*733*	*n.o.*	0.01	0.81
		4_1^+	1741	1.0	0.99	
		6_1^+	*349*	*n.o.*	0.00	
6650	6_2^+	4_1^+	2726	1.0	0.99	0.05
7601	7_1^+	5_1^+	*1936*	*n.o.*	0.30	2.5
		6_1^+	2285	1.0	0.69	
7954	8_2^+	6_1^+	2638	0.94(1)	0.92	0.17
		6_2^+	1304	0.07(1)	0.08	
8224	8_1^+	6_1^+	2908	1.0	0.52	5.0
		6_2^+	*1574*	*n.o.*	0.37	
		7_1^+	*623*	*n.o.*	0.11	
8778	7_2^+	5_1^+	3114	0.21(9)	0.39	0.02
		6_1^+	3462	0.79(9)	0.61	
9009	9_1^+	8_2^+	1055	0.41(3)	0.42	8.2
		8_1^+	787	0.59(3)	0.57	
9240	8_3^+	6_1^+	3924	1.0	0.88	0.03
		6_2^+	*2590*	*n.o.*	0.07	
9418	10_1^+	8_1^+	*1194*	*n.o.*	0.00	1.7
		8_2^+	1463	1.0	0.99	
9477	9_2^+	7_1^+	1876	0.10(5)	0.17	2.0
		8_1^+	1254	0.25(15)	0.07	
		8_2^+	1523	0.65(15)	0.74	
10469	9_3^+	7_1^+	*2868*	*n.o.*	0.15	0.24
		8_1^+	*2245*	*n.o.*	0.05	
		8_2^+	2515	1.0	0.70	
10677	10_2^+	8_1^+	2453	1.0	0.73	0.16
		8_2^+	*2723*	*n.o.*	0.15	
11001	10_3^+	8_1^+	*2777*	*n.o.*	0.06	0.09
		8_2^+	3047	1.0	0.23	
		9_1^+	*1992*	*n.o.*	0.70	
11420	11_1^+	9_1^+	2412	0.44(7)	0.24	0.10
		10_1^+	2002	0.56(7)	0.76	
11866	10_4^+	8_1^+	2626	0.20(7)	0.17	0.08
		8_2^+	3912	0.80(7)	0.35	
		9_1^+	*2857*	*n.o.*	0.12	
		9_2^+	*2389*	*n.o.*	0.17	
12359	12_1^+	10_1^+	2940	0.75(3)	0.86	0.17
		10_2^+	1681	0.25(3)	0.12	
12758	12_2^+	10_1^+	3340	0.83(7)	0.64	0.27
		10_2^+	2081	0.17(7)	0.20	
		11_1^+	*1338*	*n.o.*	0.08	
13505	12_3^+	10_1^+	*4087*	*n.o.*	0.20	0.10
		11_1^+	2086	0.62(8)	0.56	
		12_1^+	1146	0.38(8)	0.00	
13505	13_1^+	11_1^+	2086	0.62(8)	0.65	0.27
		11_2^+	*1801*	*n.o.*	0.24	
		12_1^+	1146	0.38(8)	0.11	
13644	12_4^+	10_1^+	4226	1.0	0.66	0.12
		10_2^+	*2967*	*n.o.*	0.05	
		10_3^+	*2643*	*n.o.*	0.15	
14736	14_1^+	12_1^+	2377	1.0	0.63	0.16
		12_2^+	*1978*	*n.o.*	0.24	
		13_1^+	*1231*	*n.o.*	0.12	

[a] Taken from ref. [18].

ratios match, the experimental and theoretical levels were associated with each other. This procedure was repeated towards the ground state.

The general agreement between the experimental and theoretical branching ratios is very good, and the theoretical predictions may even give confidence in some tentative spin-parity assignments of experimental levels. For example, the predicted yrast 3^+ state yields the best agreement with the experimentally observed $I^\pi = 3^+, 5^+$ level at 4932 keV, in particular considering the experimental branching ratio taken from ref. [18]. This is noteworthy because of the negative-parity assignment given in ref. [17], and because doubly magic nuclei usually have a low-lying 3^- yrast state with an excitation energy less than or similar to the yrast 4^+ state. With the present results taken in conjunction with ref. [18] there is no relatively low-lying 3^- candidate left in ^{56}Ni.

The experimental 5665 keV level is assigned a spin of $I = 5$ based on its R_{30-83} ratio and yrast arguments. The calculated 5_1^+ level has an energy of 5463 keV (including the BES shift), making it very likely that the experimental 5665 keV level indeed has a spin and parity of 5^+. In table 2 a perfect agreement between the experimental and theoretical branching ratios can be seen, *i.e.*, the two states are associated with each other. The weakly populated experimental level at 6522 keV has no spin or parity assigned. Furthermore, the calculation does not provide an adequate level. Possibly it has a negative parity and thus lies outside the model space of the calculation. Therefore, it is not included in table 2.

Another level to discuss explicitly is the 13505 keV state, which has a tentative $I = 12$ assignment, with unidentified parity. In table 2 it is compared to the predicted 12_3^+ state which correctly predicts the main branch

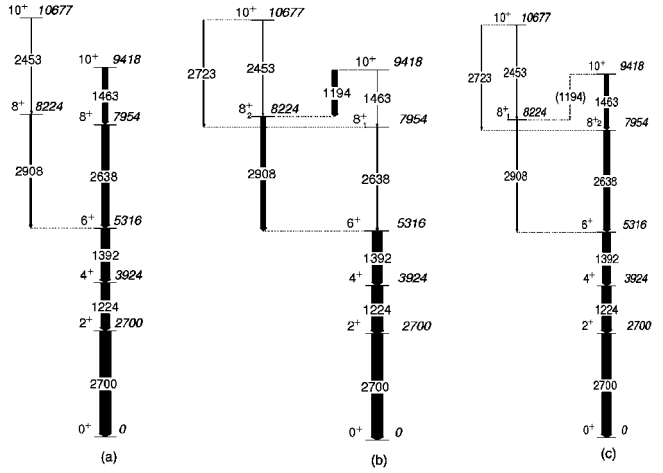

Fig. 7. Panel (a) displays the relevant part of the experimental level scheme and panel (b) shows the decay pattern as given by the shell model calculation. To the very right, panel (c) illustrates the level scheme obtained when the yrast experimental 8^+ state is associated with the second calculated 8_2^+, and vice versa. See text for details.

of the 2086 keV γ-ray, but fails for the observed 1146 keV line and predicts instead a high-energy transition into the yrast 10^+ state. Given the fact that the yrast band in general is well reproduced, one notes that the 13505 keV level is close in energy to the calculated 13_1^+ state. Interestingly, its predicted decay pattern fits the observation somewhat better (see table 2). As was discussed previously, the spin-parity assignments of rapidly decaying states can be troublesome. Indeed, the calculation indicates that this state should decay quite fast ($\tau < 0.1$ ps), which may bring into question the tentative $I = 12$ assignment of the 13505 keV state. The experimental yrare 2^+ and 4^+ states belong to a deformed rotational band, found to be based upon a 4p-4h configuration [6]. For a detailed discussion of the band the reader is referred to ref. [6].

The most interesting feature of the calculation is its inability to reproduce the feeding and decay patterns of the experimental yrast 8_1^+ state at 7954 keV and the yrare 8_2^+ state at 8224 keV. On the left-hand side in fig. 7, the relevant part of the experimental level scheme is shown. In the middle of fig. 7, the level scheme predicted by the shell model calculation is displayed. Clearly a big difference exists between the branching ratios from the experimental 10_1^+ and the calculated 10_1^+ state. A review of the leading configurations of the states in question unveils the likely reason. They are presented in table 3 together with all configurations which contribute more than 5%. All of the configurations have one proton hole and one neutron hole in the $1f_{7/2}$ orbit. In the 10_1^+ state both the excited proton and neutron are in the $1f_{5/2}$ orbit, while the 8_1^+ state has both nucleons in the $2p_{3/2}$ orbit. Surprisingly, the 10_1^+ state has only 4% of that partition. The 8_2^+ has a highly mixed wave function, but mainly one nucleon is in the $1f_{5/2}$ and the other in the $2p_{3/2}$ orbit. Intrinsically, an $E2$ transition from the main 10_1^+ configuration into the main 8_1^+ configuration is forbidden, because it requires $\Delta\ell = 2$

Table 3. The fractions of the dominating configurations for some prominent levels in ^{56}Ni.

State I^π	Fraction %	Configuration
8_1^+	26%	$\nu(1f_{7/2})^{-1}\otimes\pi(1f_{7/2})^{-1}\otimes\nu(2p_{3/2})\otimes\pi(2p_{3/2})$
8_2^+	7%	$\nu(1f_{7/2})^{-1}\otimes\pi(1f_{7/2})^{-1}\otimes\nu(1f_{5/2})\otimes\pi(2p_{3/2})$
	7%	$\nu(1f_{7/2})^{-1}\otimes\pi(1f_{7/2})^{-1}\otimes\nu(2p_{3/2})\otimes\pi(1f_{5/2})$
10_1^+	25%	$\nu(1f_{7/2})^{-1}\otimes\pi(1f_{7/2})^{-1}\otimes\nu(1f_{5/2})\otimes\pi(1f_{5/2})$
	7%	$\nu(1f_{7/2})^{-1}\otimes\pi(1f_{7/2})^{-1}\otimes\nu(1f_{5/2})\otimes\pi(2p_{3/2})$
	7%	$\nu(1f_{7/2})^{-1}\otimes\pi(1f_{7/2})^{-1}\otimes\nu(2p_{3/2})\otimes\pi(1f_{5/2})$

for both the neutron and proton partition. This creates the decay pattern shown in fig. 7(b). However, such a hindrance is not present for the $10_1^+ \rightarrow 8_2^+$ decay. Thus, if the experimental 8_1^+ state is connected with the second calculated 8_2^+ state, and vice versa, a nice agreement between the experimental and the theoretical level schemes is obtained: this is illustrated in fig. 7(c). To conclude, it appears that the shell model calculation places the experimental yrast 8_1^+ state as the second calculated 8_2^+ state and vice versa.

In principle the inversion of states is nothing unusual, at least if the calculated energy difference is less than the MLD value. For example, it has been observed for these states in ^{56}Ni earlier, but within a much more simplistic shell model approach [16], and thus considered less interesting. However, with the present large-scale shell model calculation the need for exchanging the two 8^+ states comes as a surprise, because the remaining part of the level scheme, even including the rotational band [6], is very well described. Moreover, the predicted energy difference between the two 8^+ states amounts to some $\sim$ 500 keV which is about twice the MLD value.

To check whether this peculiar discrepency is specific to the GXPF1 interaction, the calculations were repeated with the KB3G interaction [24], which represents the commonly used realistic interaction in the mass region. Interestingly, this calculation reveals the same demand for inversion of the 8^+ states, while the remaining parts of the decay scheme are again well described. Hence it seems some generic deficiency prevails in the parameter sets, caused by either single-particle energies or specific two-body matrix elements. Considering that the nuclear shell model is supposed to work at its best for doubly magic nuclei, this problem requires further theoretical investigations.

5 Summary and outlook

Through the present analysis, the number of known γ-ray transitions in ^{56}Ni have been more than doubled, providing a fairly "complete" excitation scheme up to 12 MeV excitation energy and spin $12\hbar$. A state-of-the-art shell model calculation has been performed, showing an overall very good agreement between theoretical and experimental level energies and decay patterns. However, by

studying the electromagnetic decay properties in detail an unexpected and peculiar inversion of the yrast and yrare 8^+ states is revealed. An understanding of this feature requires future theoretical efforts.

To further increase the knowledge of excited levels in ^{56}Ni, a low-spin investigation to find the 3^- state is essential, as it will give an opportunity to study the competition between single-particle excitations and collective modes. The high-spin rotational bands also merit further investigations, particularly considering the prompt particle decays [6,25] present in this mass region.

The authors would like to thank T. Steinhardt, M.N. Mineva, J.C. Waddington, O. Thelen, T. Rodinger and E. Ideguchi for support during the experiments. This work is supported in part by the Swedish Research Council and by the U.S. Department of Energy, office of Nuclear Physics, under contract No. W-31-10g-ENG-38(ANL).

References

1. M. Honma, T. Otsuka, B.A. Brown, T. Mizusaki, Phys. Rev. C **65**, 061301 (2002).
2. G. Kraus *et al.*, Phys. Rev. Lett. **73**, 1733 (1994).
3. Y. Yanagisawa *et al.*, in *Proceedings ENAM 98, Exotic Nuclei and Atomic Masses*, edited by B.M. Sherrill, D.J. Morrissey, C.N. Davids, AIP Conf. Proc. **455** (AIP, Woodbury, NY, 1998) p. 610.
4. K.L. Yurkewicz *et al.*, Phys. Rev. C **70**, 054319 (2004).
5. J. Blomqvist *et al.*, Z. Phys. A **322**, 169 (1985).
6. D. Rudolph *et al.*, Phys. Rev. Lett. **82**, 3763 (1999).
7. T. Mizusaki *et al.*, Phys. Rev. C **59**, 1846 (1999).
8. T. Mizusaki, T. Otsuka, M. Honma, B.A. Brown, Nucl. Phys. A **704**, 190c (2002).
9. I.-Y. Lee, Nucl. Phys. A **520**, 641c (1990).
10. D.G. Sarantites *et al.*, Nucl. Instrum. Methods A **381**, 418 (1996).
11. C. Andreoiu *et al.*, Eur. Phys. J. A **14**, 317 (2002).
12. D.G. Sarantites *et al.*, Nucl. Instrum. Methods A **530**, 473 (2004).
13. J. Ekman *et al.*, Phys. Rev. C **66**, 051301(R) (2002).
14. D.C. Radford, Nucl. Instrum. Methods A **386**, 297 (1995).
15. J. Theuerkauf, S. Esser, S. Krink, M. Luig, N. Nicolay, O. Stuch, H. Wolters, Program Tv, University of Cologne, unpublished.
16. D. Rudolph *et al.*, Eur. Phys. J. A **4**, 115 (1999).
17. H. Junde, Nucl. Data Sheets **86**, 315 (1999).
18. R. Borcea *et al.*, Nucl. Phys. A **695**, 69 (2001).
19. E. Caurier, Shell model code ANTOINE, IReS Strasbourg (1989, 2002).
20. E. Caurier, F. Nowacki, Acta Phys. Pol. **30**, 705 (1999).
21. M. Honma, T. Otsuka, B.A. Brown, T. Mizusaki, Phys. Rev. C **69**, 034335 (2004).
22. F. Nowacki, Nucl. Phys. A **704**, 223c (2002).
23. R. du Rietz *et al.*, Phys. Rev. Lett. **93**, 222501 (2004).
24. A. Poves *et al.*, Nucl. Phys. A **694**, 157 (2001).
25. D. Rudolph *et al.*, Phys. Rev. Lett. **80**, 3018 (1998).